Fracture Mechanics of Concrete and Concrete Structures -
Recent Advances in Fracture Mechanics of Concrete - B. H. Oh, et al.(eds)

Mesh dependency and related aspects of lattice models

M. Vořechovský & J. Eliáš
Brno University of Technology, Brno, Czech Republic

ABSTRACT: We study the effect of discretization of lattice models. Two basic cases are examined: (i) *homogeneous* lattices, where all elements share the same strength and (ii) lattices in which the properties are assigned to the elements according to their correspondence to three phases of concrete, namely matrix, aggregates, and the interfacial transitional zone. These dependencies are studied with both, *notched* and *unnotched* beams loaded in three point bending. We report the results for *regular* discretization and *irregular* networks obtained via Voronoi tessellation. The dependence of strength is compared to various size effect formulas, and we show that in the case of homogeneous lattices, the fineness of discretization of the specimens of the same size can mimic variations in the size of lattice models with the same discretization density. In the case of heterogeneity (ii), we report how both the peak force and fracture energy depend on the mesh resolution.

1 INTRODUCTION

Lattice models are well established tool for fracture modeling and they appear to be very helpful especially thanks to the increasing power of modern computers. In classical lattice models, the material is represented by a set of discrete elements interconnected by springs. The combination of simple constitutive models with a material structure incorporated from the meso-level (Lilliu & van Mier 2003, Bolander et al. 1998) or by randomness of material parameters which somehow mimics this structure (Grassl & Bažant 2009, Alava et al. 2008) makes it a powerful tool able to model quasibrittle structural response. It is an alternative to relatively complex constitutive laws applied in classical continuum models. The simplest models are those involving only elasto-brittle springs. This type of model is studied in this contribution.

The weak point of using purely brittle springs is strong dependency of the results on a network density. Since the network does not represent any real underlying structure, this dependency is understood as a bias which should be removed. If one insists on keeping the brittleness of elements as we do (no softening of elements is incorporated), the mesh size dependency can be overcome e.g. by scaling the strength of elements according to their lengths and a chosen internal length parameter (Jagota & Bennison 1995) or, as is believed, by incorporating the material inhomogeneities (voids, grains, microcracks) that introduces an internal length as well.

In this paper, we study both homogeneous and heterogeneous lattice models. By *homogeneous* models, we mean a lattice in which all elements share the same deterministic material strength criterion (and elastic modulus E). Otherwise, there are several ways to represent *disorder* or *heterogeneity* of material. This can be achieved e.g. (a) by spatial randomization of the properties of elements or, (b) by attributing element properties depending on their phase which is obtained by projecting a granular structure on the mesh. From here on, *heterogeneous* models are those obtained by alternative (b), i.e. by projecting the simulated meso-level material structure on the network and changing the properties based on the phase classification.

Both types of models can be used with either *regular* (structured, REN) or *irregular* (IRN) *geometry of the network* (or mesh). In this paper, we use both types of discretization. If we speak of structured network (REN), we use unstructured meshes with a *regular mesh* in a certain small region of interest.

In this work, we focus on the effect of varying the network density (or mesh density) on the overall structural response. We consider that *varying the network density* in homogeneous models corresponds to changes in *structural size* of the structure modeled. In other words, by changing the network density, we might model different sizes of the specimen.

Several papers concerning the effect of network density have been published but, according to authors' knowledge, two issues have not been studied yet: (i) the effect of size on the strength of the *homogeneous* model with a *random* network geometry (IRN) and, (ii) the effect of grain microstructure projected on the specimen with varying network densities (the grain layout properties to be used to classify elements is kept, but the network density – mesh – is varied).

These mesh-density effects are studied for both: specimens that fail by crack initiated from a smooth surface and notched specimens. In particular, we have performed numerous simulations with either notched or unnotched three-point-bent specimens (denoted either nTPBT or uTPBT). The geometry of the specimens is illustrated in Figure 1 top. The span $S=3D$ is equal to three times the specimen depth D.

We have found this topic interesting because the irregularity of the network influences the strength unexpectedly. Not all the sources of the observed behavior were identified and analytically analyzed, thus, the contribution predominantly present our (mostly numerical) observations.

The first part of the contribution describes briefly the model adopted. The following sections (3 – 6) are devoted to the observed size effects in *homogeneous lattice models with* both REN and IRN. The last part presents a short study describing how (whether) the meso-level concrete structure projected onto the model reduces these size (or mesh density) effects.

2 BRIEF DESCRIPTION OF THE MODEL

2.1 *Mechanics of discrete model*

Several lattice-type models can be found in literature. Here, the *rigid-body-spring network* developed by Kawai (1978) is used. In basics, the model is very similar to the one published by Bolander & Saito (1998). The fracture criteria are taken from the same article, i.e. Mohr-Coulomb surface with tension cut-off is adopted. More detailed description can be found in Eliáš (2009). In this paper, we study models with missing rotational springs at the connection of adjacent facets. If so, only normal and shear springs transfer the internal forces.

As mentioned above, in the case of *homogeneous* models, the strength criterion defined by the breaking stress is identical for all springs. Tensile strength of all elements is set to 5 MPa. Also the E-modulus is the same for all springs.

Forces carried by springs are influenced by the corresponding cross-sectional area A, spring length l and Poisson ratio. The cross-sectional area is calculated from the contact area between the rigid bodies (Fig. 1). The springs representing the contact areas operate on the actual eccentricity coming from the discretization.

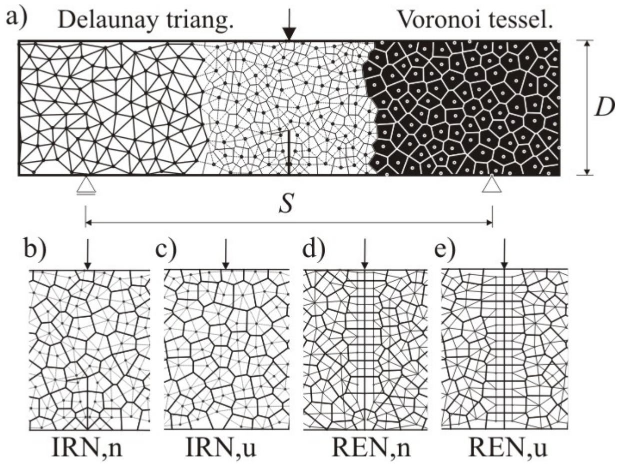

Figure 1. Specimens with a central notch: nTPBT (relative notch depth α=1/3). Two types of meshes around a notch are presented: REN and IRN. The Delaunay triangulation corresponding to the dual graph of the Voronoi tessellation is illustrated for a given mesh density. The configuration of uTBPT is identical except for the missing notch.

2.2 *Meshing algorithm*

It has been proven by several authors (e.g. Schlangen & Garboczi 1997, Jirásek & Bažant 1995) that irregular geometry of the network helps to avoid directional preference of crack propagation. Thus, it has been chosen for the present model.

The meshing algorithm is based on Voronoi tessellation, which is performed on the set of pseudo-randomly placed triangulation nodes within the domain. The only restriction is that their minimal mutual distance equals to a predefined parameter $l^{\min}$.

When a notch is to be modeled, it is included by mirroring nodes by the notch line in the notch vicinity, see Figure 1 b and d. Voronoi tessellations then creates a straight line and all springs on that line are subsequently removed to model the notch. In order to place the notch tip exactly at the desired coordinate, three points are placed with a prescribed distance from the tip. This procedure guarantees an exact location of the shared vertex – the interface of the three corresponding rigid bodies at the notch tip.

2.3 *Deviations from the theory of elasticity*

The stiffness of springs is derived to represent an underlying imaginary isotropic, linearly elastic homogeneous continuum (Kawai 1978).

However, the elastic behavior differs from the assumed theory. The effect is clearly described by Schlangen & Garboczi (1996). Simply, the isotropic elastic material should exhibit uniform stress under uniform strain. Voronoi tessellation can satisfy this criterion for zero Poisson's ratio ν. However, as showed by Bolander et al. (1999), for nonzero Poisson's ratios, the stress distribution of a body under remote uniform uniaxial strain is not uniform any more. The greater the deviation from zero ratio ν, the more fluctuation in stress occurs (see error bars in Fig. 2).

We also observed that Poison's ratio severely influences the stress in the surface layer of elements. The average values of stresses in the lowermost elements of uTPBT diverge from the linear stress profile approximately obtained for zero ratio ν (Fig. 2). Elsewhere, the average stresses roughly correspond to ν=0.

That is why unnotched (uTPBT) specimens with a positive Poisson's ratio tend to yield nominal strengths lower than the prescribed overall direct tensile strength. The explanation can be put in the following words: locally there is a greater stress σ^{∞} at the bottom face compared to that of isotropic homogeneous continuum. This strength drop will be visible in results of our simulations (Fig. 8).

There is no effect observed of Poisson's ratio on strength in the case of notched specimens (nTPBT).

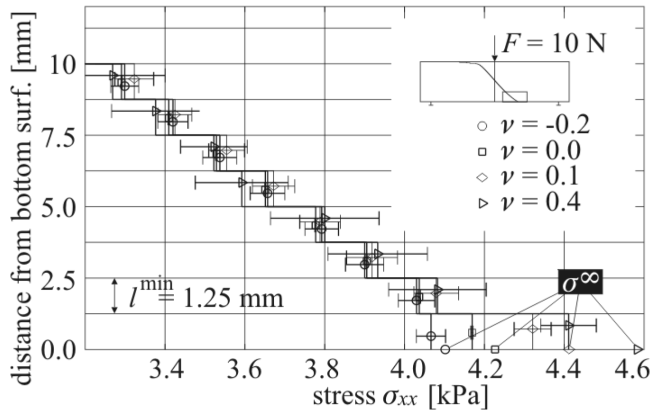

Figure 2. Effect of poisons ration on stresses σ_{xx}. Figure shows the lowermost part of stress profile of uTPBT with regular net geometry loaded by force 10 N. Error bars shows averages and sample standard deviations computed from 50 realizations.

3 SIZE EFFECT SIMULATIONS

The size of a concrete specimen typically affects the observed nominal strength. Several sources of this phenomenon are documented (Bažant & Planas 1998), we name the statistical and deterministic effects. Two main types of the deterministic size effects are distinguished. Structures with preexisting notches (positive geometry exhibiting type II size effect) and structures without any notch or with a small notch with respect to material internal length (negative geometry exhibiting type I size effect).

Notched (type II, nTPBT) and unnotched (type I, uTPBT) are used to study this size effect in *homogeneous* brittle-spring networks. The density of the network is denoted as $l^{\min}$. Since there is no internal length in our constitutive law/model, we can represent varying size by varying network density. The characteristic size (depth) D is kept constant at a reference size D_0 = 0.1 m, whereas the network density $l^{\min}$ is varied; and we can mimic varying of the *intrinsic* size D by writing:

$$D = D_0 \frac{l_0^{\min}}{l^{\min}} \tag{1}$$

where $l_0^{\min}$=0.02 m is the selected reference mesh density.

Since we deal, in fact, with models of the same size, it is not necessary to report the size dependence on nominal strength (nominal stress at peak load). It suffices to report the loading forces F (D). On the other hand, however, the lengths (e.g. crack length) must be recalculated in a similar fashion as we did for D (see Equation 1). Removal of one element of the same size is interpreted as a crack of different lengths in models of various mesh densities.

In order to evaluate the effect of network *irregularity*, all the results are computed for REN and IRN.

Since the network in REN models is only regular in the vicinity of notch or midspan, the rest of the specimen (meshed by a lattice of irregular geometry) causes fluctuations of forces acting on the "crack faces". Subsequently, the obtained nominal forces are scattered. This effect is emphasized in unnotched structures, see e.g. Figure 7.

In the regular networks, the rupture of the first element (beam or spring) causes the collapse of the whole structure. This holds both in the nTPBT and uTPBT. Therefore, the measured *peak loads* F^p equal the *elastic limits* F^e in the case of REN.

4 SIZE EFFECT OF NOTCHED STRUCTURE

In the case of *regular mesh* geometry (REN), the crack can only propagate along the axis of symmetry through regularly placed squared elements of *exact* size $l^{\min}$. The peak forces (that are the elastic limits at the same time) of REN plotted against the net density $l^{\min}$ (or size D) in loglog plot fall exactly on a line of slope –½ (see Fig. 3). This result is not new and corresponds to the remedy of size dependency of homogeneous regular lattice models proposed by Jagota & Bennison (1995).

Network irregularity (IRN), however, brings a new effect. Since the element placed right above the notch tip is angled and has varying size, the external load F^e necessary to break it is affected. Usually, more than one element must be broken to reach the peak force F^p, i.e. $F^e < F^p$.

The elastic F^e limit obeys LEFM slope of –½ and lies very close to the previous fit with regular networks (dotted line in Fig. 4). This is surprising because two effects working one against the other appears here. (i) The angle of the first element (deviation from horizontal direction) increases the elastic limit force, i.e. shifts the line upwards. (ii) The average area of the first broken element is lower in IRN than in REN where all broken elements have the area l^{min}×thickness. This leads to downward shift of the size effect line. Apparently, effects of those the upward and downward shifts cancel each other.

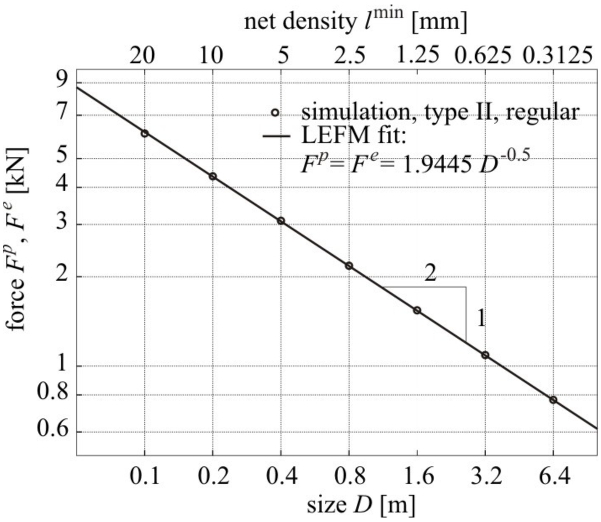

Figure 3. Simulations of nTPBT beams with regular mesh REN. Each circle is an average of 30 simulations (except for size 6.4), error bars are not included as the standard deviation is extremely small. Fitted by LEFM prediction (a straight line of slope –½).

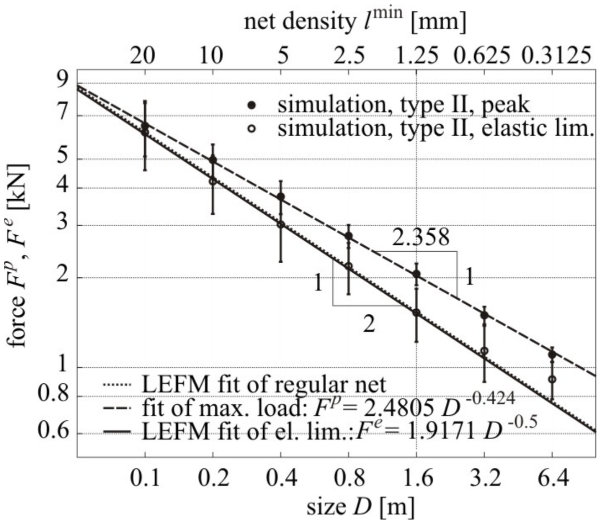

Figure 4. Simulations of nTPBT beams with irregular mesh (IRN). Each circle is an average value of 50 simulations (except for size 6.4, only 10).

Looking at the *peak force* data, the best fit in loglog plot is a straight line of slope –0.424, see Figure 4. The source of observed deviation from the LEFM slope of –½ was found in the crack behavior. Figure 5 shows crack patterns at the peak load for all considered sizes. These crack length are recalculated into the intrinsic magnitudes (Equation 1). Apparently, the larger the specimen, the longer the length at the peak load: the crack initiation from the notch is followed by an *increase in peak crack length* with size D. This increase can be fitted by a power law with exponent ½ (see Fig. 10). The slower declination of the fitted power law in Figure 4 (–0.424) can be attributed to the described growth in crack length with specimen size D.

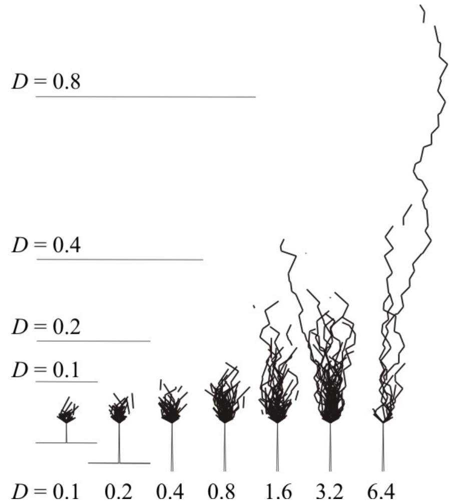

Figure 5. Crack patterns at the peak load for various sizes of the notched IRN beam (with irregular mesh geometry).

5 SIZE EFFECT OF UNNOTCHED STRUCTURE

A somewhat different situation appears when the beam fails by cracking initiating from the smooth surface (such as our uTPBT).

In our numerical simulations, the unnotched specimens have similar features to the nTPBT. In the case of regular geometry (REN), the first rupture of the beam at the bottom surface leads to collapse of the whole beam. Figure 7 shows the maximal load depending on the density of the REN net (or, the size of the structure D).

Let us now deliver a closed-form expression for the observed size effect. Consider the midspan rectangular cross-section BD. The depth is discretized into $2N$ rigid bodies' contacts of the same size, see Figure 6. Therefore the stress profile is a piecewise constant function along the depth D and approximates the actual (almost perfectly) linear profile. When the outermost spring reaches the extreme tensile stress f^{∞}, the cross-section reaches its maximum bending moment M. Due to the symmetry along the neutral axis we can consider only the lower bottom of the depth (N elements) and calculate the bending moment as a doubled sum of force contributions times the corresponding arm. Each force contribution can be written as (Fig. 6):

$$T_i = B \cdot \frac{D}{2N} \cdot \frac{i - 1/2}{N - 1/2} f^{\infty}, \quad i = 1, \ldots, N \qquad (2)$$

where B is the bar thickness [m], the second factor is the bin width $l^{min}=D/(2N)$ [m] and the third factor is the corresponding constant stress in that bin [N/m^2]. Each such a force has the following arm from the neutral axis:

$$r_i = \frac{D}{2N}\left(i - \frac{1}{2}\right), \quad i = 1,\ldots,N \tag{3}$$

where again, the first factor is the bin width. The resisting moment is a double of the sum (i=1,…,N):

$$M\left(N\right) = 2\sum_{i=1}^{N} T_i r_i = \frac{BD^2}{4N^2}\frac{f^{\infty}}{N-1/2}\sum_{i=1}^{N}\left(i-\frac{1}{2}\right)^2 \tag{4}$$

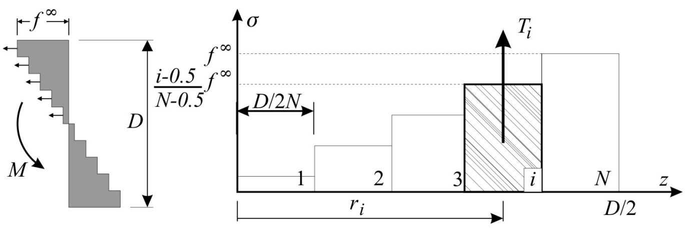

Figure 6. On derivation of the peak moment in a bent specimen.

Calculating the sum yields the following simple term in the parenthesis:

$$M\left(N\right) = \frac{BD^2}{6} f^{\infty} \left(\frac{2N+1}{2N}\right) \tag{5}$$

As N grows to infinity, the bending moment converges to the well-known value:

$$M^{\infty} = f^{\infty}\ BD^2 / 6 \tag{6}$$

The external moment equals the support reaction times the half span: $M=F/2 \cdot 3D/2$. Putting this equal to Equation (5) yields:

$$F = \frac{2BD}{9} f^{\infty}\left(\frac{2N+1}{2N}\right) \tag{7}$$

Equation (7) can be transformed into the dependence of peak force on bin width $l^{min}=D/(2N)$:

$$F_{\max} = \overbrace{\left(\frac{2BD}{9}\right)}^{c} f^{\infty}\left(1+\frac{l^{\min}}{D}\right) = F^{\infty}\left(1+\frac{l^{\min}}{D}\right)$$
(8)

This equation is plotted in Figure 7 and compared to the computed data. We can introduce a new length constant $D_b = l^{min} = 20$ mm to make it identical with Equation 10 introduced later. What remains to be clarified is the choice of the extreme stress f^{∞}. An obvious choice for would be the direct tensile strength (f_l^{∞}= 5 MPa) of the model. This is because very large specimens fail at initiation of crack right at the midspan bottom face, which must equal the tensile strength. It would yield the asymptotic force F_l^{∞} = 11.11 kN. Unfortunately, the stress profile in not perfectly linear in reality. The real stress profile is affected by wall effects (the span of the beam is only 3D) and by the local compressive stress concentration around the point load. The nonzero Poisson's ratio causes additional deviation from linear stress profile. As an approximation, we used nonlinear square fitting procedure to determine both parameters D_b and F^{∞}. One can calculate the theoretical stress at the bottom layer for infinitely small mesh caused by load 10 N, see Sec. 2.3. This stress σ^{∞} is added into Figure 2 to show consistency with our fits.

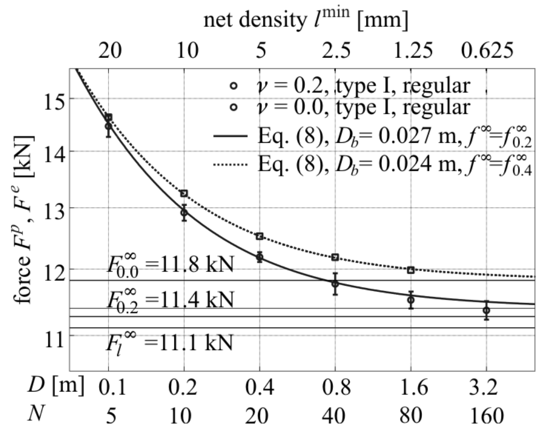

Figure 7. Dependency of peak load on the REN network density (structural size D). Comparison with the size effect formulas (Equations 8 and 10).

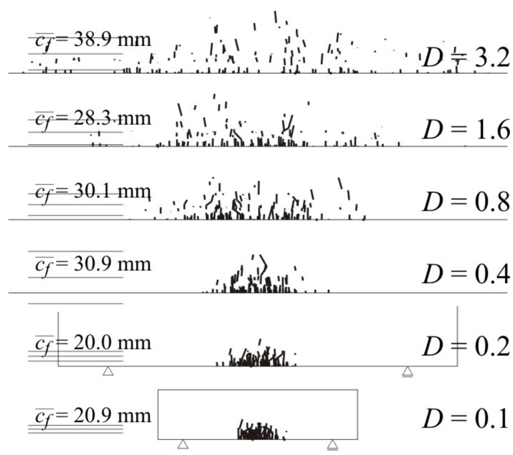

Figure 8. Crack patterns at the peak load for various sizes of the unnotched beam with irregular network geometry. Left horizontal lines indicate the average height c_f reached by the crack and its standard deviation.

Is it worth pointing that another way exists to nicely fit the data – to consider the bent specimen being made of a quasibrittle material. One can assume a linear stress profile along the depth except for the damaged zone in the bottom tensile part. If we consider that the boundary layer of cracking has a constant size c_f irrespective the specimen size, the following size effect formula can be derived (see pages 41-43 of Bažant 2005) for scaling of nominal strength (modulus of rupture):

$$\sigma_N = f_r\left(D; f^{\infty}, D_b, r\right) = f^{\infty}\left(1 + \frac{rD_b}{D}\right)^{1/r} \qquad (9)$$

where f^{∞} is the strength limit for infinitely large structures and $D_b = 2\ c_f$, i.e. double of the thickness of the boundary layer of cracking. If we take r=1 which is a special case derived by Bažant and Li (1995), and rewrite Equation 9 in forces:

$$F_{\max} = \underbrace{\overbrace{\left(\frac{2BD}{9}\right)}^{c} f^{\infty}}_{F^{\infty}}\left(1 + \frac{D_b}{D}\right) = F^{\infty}\left(1 + \frac{D_b}{D}\right) \qquad (10)$$

When $D_b = l^{\min}$, this formula is identical to Equation 8 derived here using different arguments.

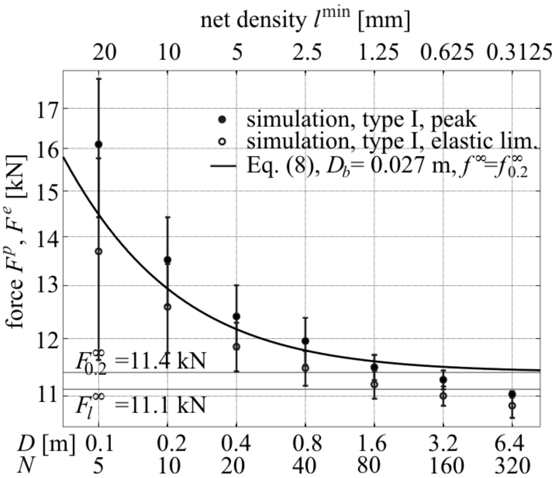

Figure 9. Elastic limits and peak loads of beams with IRN network and smooth bottom surface. Average values and standard deviations are estimates from 50 realizations for every size.

The irregularity of the network geometry (IRN) allows the model to choose the "weakest" area to initiate and propagate the crack. That is why the elastic limits are, on average, lower in IRN compared to REN, see Figure 9. The load applied to break the first spring F^e in IRN model is, on average, also much lower than the peak forces.

The peak forces in IRN models are greater than those of REN. The first crack appears at the weakest spring loaded by high forces: the crack prefers short springs (the minimum length of which is $l^{\min}$). Qualitatively, however, both force dependencies of IRN are similar to REN and follow the tendency proposed by Equation (8). The deviations for larger specimens are caused again by local stress deviations described in Section 2.3. Namely, we mean the stress fluctuations caused by Poisson's ratio in the lowermost layer. These cause earlier ruptures then expected in isotropic homogeneous media (tensile strength of 5 MPa). Both the elastic forces and peak forces can drop below this horizontal asymptote; see Figure 9.

Instead of one crack, many small cracks are created inside the bottom area of the specimen (Fig. 8) and the model allows for redistribution of forces after many such local ruptures. These cracks do not form a continuous line.

On average, the thickness of the boundary zone of distributed cracking is > $l^{\min}$. The fact that the zone has approximately the same height for all sizes (Fig. 8), supports our claim that the data can be approximated reasonably well by Equations (8 and 10).

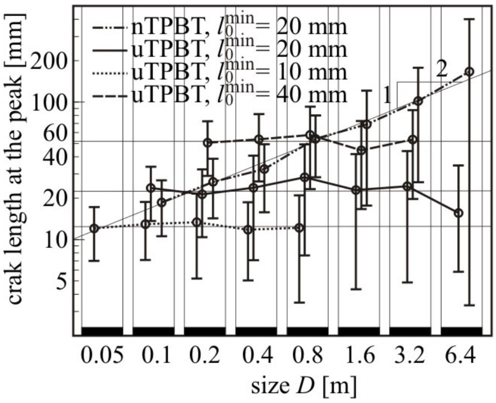

Figure 10. Length of the crack at the peak load for notched and unnotched TPBT.

6 DISCUSSION

Some interesting points have been shown in the two preceding section and we now discuss some of the features in a more detail.

It was mentioned previously that the length of a crack at the peak load seems to be increasing in the nTPBT IRN simulations while the average crack length at the peak load is about constant in uTPBT, see Figures 5 and 8.

Surprisingly, the increase in the crack length of IRN nTPBT specimens obeys a power law with exponent ½ (see the thin angled line in Fig. 10).

In the case of unnotched specimens, the constant peak crack length is dependent on reference network density $l_0^{\min}$. This was checked numerically by additional simulations with various lengths $l_0^{\min}$ (otherwise kept constant here); see the thin horizontal lines in Figure 10 which shows that the average peak crack length roughly lies in the range of 1.1-1.3 $l_0^{\min}$. In conclusion, scaling both the network size and the specimen size by the same positive scaling factor yields an identical result as for the original sizes. The peak force depends only on the quality of the stress profile approximation.

We have performed a sensitivity analysis to identify the influence of various parameters on the elastic limit load and the peak load. In particular, Spearman nonparametric correlation coefficient was used. The greatest absolute correlation to the peak load was found with the maximum vertical coordinate of the crack – i.e. the thickness of the zone with distributed cracking c_f. In the case of notched specimens, the elastic limit force F^e is sensitive to the initial crack length as well as to the inclination of the initial crack from vertical direction (corr. coeff. approx. 0.8). Unfortunately, no dominant variable which affects the peak load was identified.

Let us also mention recent results of Alava et al (2008) who show, using random fuse model, that strength of notched beams of various *sizes* and notch depths is influenced by the amount of disorder. The strength dependence on notch depth deviates from LEFM power law with an increasing disorder. Specimen strength made of highly disordered material, with a small notch, is driven mainly by the disorder and not only by the stress concentration.

7 REDUCTION OF SPURIOUS SIZE EFFECT

The influence of network density has to be understood as a spurious phenomenon, because the mesh is arbitrary, artificial and does not arise from any real material structure. Some authors believe that the network density dependency might be removed by projecting the material inhomogeneities onto the lattice. This introduces the internal length, which decrease this dependency (van Mier & van Vliet 2003). In the following, this expectation is subjected to critical study, which shows limits of such a procedure.

7.1 *Incorporating of grain structure*

The grain structure that is used here is generated by computer algorithm using the Fuller curve (see e.g. Cusatis et al. 2006). Typically, maximal grain diameter d_{max} is chosen according to real batch contents, and the minimal d_{min} according to the network density. The length of network elements should be at least three times smaller than d_{min} (van Mier 1997), otherwise the particles coalesce in the mesh.

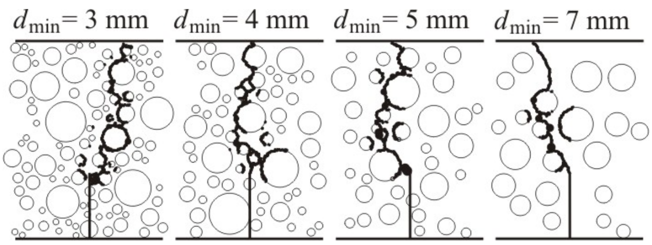

Figure 11. An example of crack patterns observed in a simulation of notched TPBT with the model including concrete mesoscopic grain structure of varying fineness.

Grains smaller than d_{min} are ignored in the procedure. The larger d_{min}, the coarser mesoscopic structure is incorporated; yet, the generated coarse grains still correspond to the requested content of coarse grains, i.e. reducing d_{min} has no effect on coarse grains – it only adds finer aggregates.

Grains were projected onto the lattice to attribute springs with the three material phases – aggregate, matrix and ITZ. These are distinguished according to positions of nodes with respect to the mesostructure (see e.g. van Mier et al. 1997). Each phase has a different strength and Young's modulus. Values from the article by Prado & van Mier (2003) were used.

In the following part, we will test the hypotheses that the finer the mesoscopic structure is considered, the lower mesh sensitivity is observed. For this reasons, six different grain contents were generated. The first one is the *homogeneous* case without any grain (studied above), the other differ by d_{min} (Fig. 11) whereas maximum grain diameter d_{max} is kept equal to 32 mm.

Mesh varied from density 2.5 mm up to density 0.625 mm. Note that not all the densities can be used for all the grain contents. The finer grains, the finer mesh is required. For all possible combinations, 50 realizations of notched TPBT were simulated.

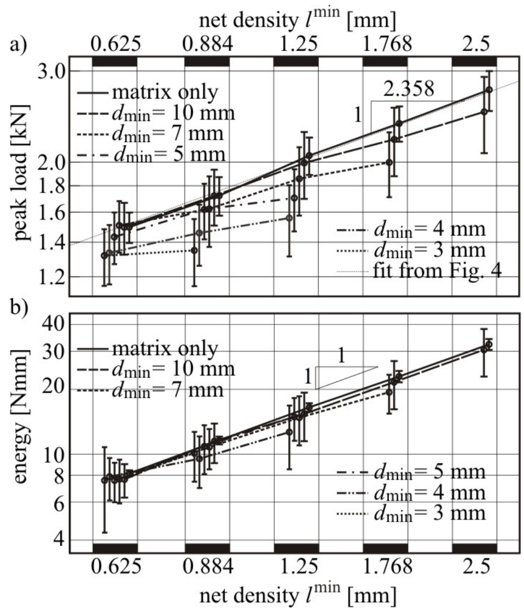

Figure 12. Dependency of (a) maximum load and (b) area under load-deflection curve on network density for various grain contents.

In order to have an idea about the model behavior, Figure 13 shows average load-deflection diagrams for some of considered densities and mesostructures.

The results for the peak loads are shown in Figure 12a. The homogeneous model follows a straight line of slope 0.424 (previously described in Fig. 4).

Models with grain contents seem to reduce this dependency. The best results (almost a horizontal line) are achieved by the most detailed grain contents. The second monitored parameter is the area under load-deflection curves, which has meaning of energy. Unfortunately, no reduction in the dependence of this energy on mesh density was observed. Figure 12b documents that all the lines share approximately the same slope of 1.

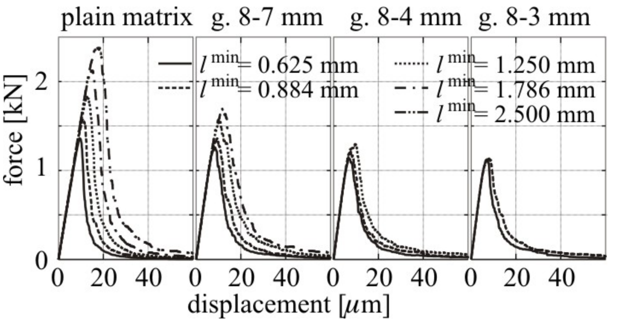

Figure 13. Average load-deflection diagrams of 50 nTPBT for some of considered densities and mesostructures.

8 CONCLUSIONS

The effect of discretization of lattice models was studied. The basic cases are examined: (a) homogeneous lattices, where all elements share the same strength and (b) lattices in which the properties are assigned to the elements according to their correspondence to three phases of concrete, namely matrix, aggregates, and the interfacial transitional zone (ITZ). These dependencies are studied with both, notched and un-notched beams loaded in three point bending. We report the results for regular discretization and irregular networks obtained via Voronoi tessellation. The dependence of strength is compared to various size effect formulas and we show that in the case of homogeneous lattices, the fineness of discretization of the specimens of the same size can mimic variations in the size of lattice models with the same discretization. In the case of heterogeneity (b), we report that even though the peak force dependence on the mesh resolution disappears, a strong dependence of the fracture energy remains.

ACKNOWLEDGEMENTS

This outcome has been achieved with the financial support of the Czech Ministry of Education, Youth and Sports, project MSMT 0021630519 and also of Czech Science Foundation, project GACR 103/09/H085 were partially exploited. The second author acknowledges the support from the Fulbright commission within the framework of Fulbright-Masaryk fellowship.

REFERENCES

Alava, M.J., Nukala, P.K.V.V & Zapperi, S. 2008. Fracture size effects from disordered lattice models. International Journal of Fracture 154: 51–59.

Bažant, Z.P. (2005). Scaling of Structural Strength; 2nd updated ed., Elsevier Butterworth-Heinemann

Bažant, Z.P. & Li, Z. (1995). Modulus of rupture: size effect due to fracture initiation in boundary layer. J. of Struct. Engrg – ASCE, 121(4): 739–746.

Bažant, Z.P. & and Planas, J. 1998. Fracture and Size Effect in Concrete and Other Quasibrittle Materials. CRC Press, Boca Raton and London.

Bolander, J.E., Hikosaka, H. & He, W.-J. 1998. Fracture in concrete specimens of different scale. Engineering Computations 15: 1094–1116.

Bolander, J.E. & Saito, S. 1998. Fracture analyses using spring networks with random geometry. Engineering Fracture Mechanics 61: 569–591.

Bolander, J.E., Yoshitake, K. & Thomure, J. 1999. Stress analysis using elastically homogeneous rigid-body-spring networks. Journal of Structural Mechanics and Earthquake Engineering 633: 25–32.

Cusatis, G., Bažant, Z.P. & Cedolin, L. 2006. Confinement-shear lattice CSL model for fracture propagation in concrete. Computer Methods in Applied Mechanics and Engineering 195: 7154–7171.

Eliáš, J. 2009. Discrete simulation of fracture processes of disordered materials. Ph.D. thesis, Brno University of Technology, Faculty of Civil Engineering, Brno, Czech Republic.

Grassl, P. & Bažant, Z.P. 2009. Random lattice-particle simulation of statistical size effect in quasi-brittle structures failing at crack initiation. Journal of Engineering Mechanics 135: 85–92.

Jagota, A. & Bennison, S. J. 1995. Element breaking rules in computational models for brittle materials. Modelling and Simulation in Materials Science and Engineering 3: 485–501.

Jirásek, M. & Bažant, Z.P. 1995. Particle model for quasibrittle fracture and application to sea ice. Journal of Engineering Mechanics 121: 1016–1025.

Kawai, T. 1978. New discrete models and their application to seismic response analysis of structures. Nuclear Engineering and Design 48: 207–229.

Lilliu, G. & van Mier, J.G.M. 2003. 3D lattice type fracture model for concrete, Engineering Fracture Mechanics 70: 927–941.

Schlangen, E. & Garboczi, E.J. 1997. Fracture simulations of concrete using lattice models: computational aspects. Engineering Fracture Mechanics 57: 319-332.

Schlangen, E. & Garboczi, E.J. 1996. New method for simulating fracture using an elastically uniform random geometry lattice. International Journal of Engineering Science 34: 1131–1144.

Prado, E.P. & van Mier, J.G.M. 2003. Effect of particle structure on mode I fracture process in concrete. Engineering Fracture Mechanics 70: 1793–1807.

van Mier, J.G.M. 1997. Fracture Processes of Concrete: Assessment of Material Parameters for Fracture Models. CRC Press, Boca Raton, Florida.

van Mier, J.G.M. & van Vliet, M.R.A. 2003. Influence of microstructure of concrete on size/scale effects in tensile fracture. Engineering Fracture Mechanics 70: 2281–2306.

van Mier, J.G.M., Chiaia, B.M. & Vervuurt, A. 1997. Numerical simulation of chaotic and self-organizing damage in brittle disordered materials. Computer Methods in Applied Mechanics and Engineering 142: 189-201.